On the Inflection Point Instability of a Stratified Ekman Boundary Layer

R. A. BROWN[1]

National Center for Atmospheric Research,[2] Boulder, Colo. 80302

(Manuscript received 15 July 1971, in revised form 28 February 1972)

ABSTRACT

The neutral Ekman boundary layer is known to be dynamically unstable to infinitesimal perturbations under typical geophysical conditions. This paper discusses this instability to two-dimensional, simple-harmonic perturbations, for the stratified Ekman layer.

While viscosity and Coriolis forces are generally important in setting up the basic mean profile, the inflection point instability can be investigated in the inviscid, non-rotating system limit. However, the singular nature of the resulting second-order characteristic equation makes it necessary to solve the non-singular sixth-order, viscous stratified equation. Since typically occurring Reynolds numbers are much larger than critical, emphasis has been placed on investigating the behavior of maximum growth rates versus stratification for large Re. The appropriate dimensionless parameters are found to be: $\xi=(2/\mathrm{Ro\ Re})^{\frac{1}{2}}$, and $\mathrm{Ra}=gS\delta^4/K_mK_h$ [where $\delta=(2K/f)^{\frac{1}{2}}$, $\mathrm{Re}=V_g\delta/K_m$, $\mathrm{Ro}=V_g/f\delta$ and $S=(\bar{T}_z+g/c_p)/\bar{T}$] for the general case, or ξ and $\mathrm{Ri}=gS/V_z^2$ for the inviscid case.

Unstable stratification shifts maximum growth rates toward a longitudinal orientation and shorter wavelengths from the neutral stratification values of leftward orientation angle, $\epsilon=17°$, and wavenumber, $\alpha=0.5$. The local Richardson number at the inflection point is found to be the pertinent parameter for the effects of stratification. This instability is damped completely for values of $\mathrm{Ri}_l>0.25$. Unstable stratification tends to support the dynamic instability such that the growth rate for this mode is dominant significantly into the convective instability regime.

The instability takes the form of counter-rotating circular motions which remain qualitatively similar for a wide range of the basic variables.

1. Introduction

There exists ample evidence of mesoscale wave structure in the planetary boundary layer and elsewhere in the atmosphere and the ocean. In the atmosphere, these waves are characterized by two-dimensionality, wavelengths from 0.5 to 10 km, or frequencies from 15 min to 2 hr, and uniformity over areas from several wavelengths to hundreds of kilometers. In particular, they are longitudinal waves, orientated with axes approximately parallel to the mean wind.

There also exist many theories predicting these waves, as diverse as: 1) topographically oriented convective plumes, which falls short of explaining the abundant observations over uniform terrain; 2) second-order longitudinal vortices induced by the nonlinear interaction of the first-order disturbance, which considers the growth of instabilities near the critical (minimum) Reynolds number in a plane shear flow (Benny, 1960); and 3) the tendency of wind shear to cause the purely convective instability to favor a longitudinal distribution model (Ogura and Yagihashi, 1969).

While it is probably not possible at this time to resolve any particular mechanism as *the* cause of observed atmospheric secondary motions, there are sufficient observations to indicate that although these waves are most commonly observed in slightly unstable stratified conditions (LeMone, 1972), they are also present when the fluid is neutrally stable and possesses either very little or no speed shear. The few cases observed with no speed shear were found in the lower troposphere and possessed turning velocity profiles. On the mesoscale and larger, the Coriolis forces are significant and act to turn the wind, and the turning profile can present a velocity profile with an inflection point instability to properly oriented two-dimensional perturbations. Since the geophysical Reynolds numbers are supercritical by at least an order of magnitude, primary attention in this paper is given to the effect of stratification on the maximum growth rate of this dynamic instability in the planetary boundary layer.

The derivation of the complete stratified, rotating, viscous stability equations is included with particular attention to the non-dimensionalization of these equations. This is done with the hindsight that the entire eighth-order set is either unnecessary or too unwieldy for solution at this time. Hence the equations obtained in various limits should be investigated. It is concluded

[1] Present affiliation: Department of Atmospheric Sciences, University of Washington.

[2] The National Center for Atmospheric Research is sponsored by the National Science Foundation.

Unauthenticated | Downloaded 08/03/24 07:12 AM UTC

that the inviscid non-rotating limit qualitatively describes the dynamic instability mode, although the addition of viscous terms are necessary from a mathematical standpoint.

The analytic status of the stability equation including stratification and viscosity was discussed by Miles (1960). Koppel (1964) has discussed the equations for a parabolic $V(z)$ including the Boussinesq approximation. These analyses considered asymptotic solutions, revealing the importance of the critical layer at $U=C_r$, and stability for $\mathrm{Ri}>0.25$. Stratified Couette flow was investigated numerically by Gallagher and Mercer (1965) and the stratified Poiseuille flow case has been discussed generally by Gage and Reid (1968), delineating the neutral stability boundaries. Asai (1969) has numerically investigated thermal convection in the presence of parallel shear flows including Couette and Poiseuille profiles, and an arbitrary profile exhibiting an inflection point. In the last case, the inflection point instability apparently appeared in conjunction with the thermal instability. Recently, Maslowe and Thompson (1971) have also performed numerical stability calculations for an arbitrary stratified parallel flow with an inflection point. These studies have all indicated the stabilizing effect of shear on the convective mode, and the generality of the $\mathrm{Ri}>0.25$ criterion for stability. In particular, the Rayleigh/Bénard criteria for convective instability appear, independent of shear, for two-dimensional perturbations oriented perpendicular to these parallel flows (hence, longitudinal waves).

Ekman layer instability with thermal stratification and Coriolis forces was investigated for the critical (minimum) Reynolds number region, using finite differencing, by Etling (1971). He found the Coriolis terms, including the vertical component, to be important to the determination of the neutral stability region on a wavenumber vs Reynolds number plot ($\mathrm{Re}<500$). The damping effect of stable stratification was found to be much greater on the inflection point mode than on the "parallel" mode, which continued to exist in very stable mean stratifications. The latter mode was found by Lilly (1966), and found to be dependent on the Coriolis terms.

Kaylor and Faller (1972) have investigated the stably stratified Ekman layer using finite differencing of the time-dependent Navier-Stokes equations. They have found an instability region in the stably stratified domain, which they attribute to a resonance between instability waves and internal gravity waves. Although the Coriolis forces are essential to the transfer of energy from longitudinal perturbations to lateral perturbations, the sources of the energy remain speculative.

In the case of the Ekman layer, there exist different shear profiles for all two-dimensional perturbations over a 180° range (the remaining 180° presents a symmetric set). Thus, the dynamic instability can be expected to vary with the nature of the inflection point while the convective instability varies in relation to the shear profile in general.

The dynamic instability is found to be completely damped when Ri_l at the inflection point is greater than a small positive value which has a maximum value of 0.25. With the addition of buoyancy forces in the negative Ri region, the expected amplification of growth rates in the dynamic instability are found. In addition, the growth of the purely convective mode can be expected to eventually dominate as Ri decreases. However, this mode is modulated by the shear such that the dynamic instability growth rates may remain greater for moderately unstable values of Ri.

One of the problems in the presentation of this analysis is the proliferation of independent variables. The stability must be investigated *a priori* as a function of Reynolds number Re or ξ, Rayleigh number Ra, Prandtl number Pr, bulk or local Richardson number Ri or Ri_l, Rossby number Ro, orientation angle ϵ, roughness parameter δ, and wavenumber α. This number of parameters can be reduced using the self-similarity of the Ekman profile with respect to δ, and the subsequent relationships, $\mathrm{Ro}=\mathrm{Re}/2$, and $\mathrm{Ra}=\mathrm{Re}^2\mathrm{Pr}\ \mathrm{Ri}$. In addition, consideration of the non-dimensional equations suggests a weak dependence on Ra, Re and Pr. These indications are confirmed in the results, together with the preference for Ri_l rather than the bulk Richardson number. Since the growth rates still depend upon Re, Ri, ϵ and α, graphical presentation requires fixing some parameter either with a realistic physical value or a relatively constant value (e.g., the inflection point mode is relatively independent of Re for $\mathrm{Re}>500$). For these reasons, and indications that the convective and dynamic instabilities may coexist, the discussion of this paper is restricted to the effect of stratification upon the inflection point instability, leaving the complete exploration of the convective mode to a subsequent analysis.

2. Development of the general equations

a. Basic equations and non-dimensionalization

Consider the Navier-Stokes equations with the rotation terms and the constant eddy coefficients, K_m and K_h (an overhead dot indicates the substantive derivative):

$$\left.\begin{aligned} \dot{\mathbf{V}}+2\boldsymbol{\Omega}\times\mathbf{V}+\nabla p/\rho+g\mathbf{k}-K_m\nabla^2\mathbf{V}=0 \\ \dot{\rho}+\rho\nabla\cdot\mathbf{V}=0 \\ \dot{T}+(p/\rho c)\nabla\cdot\mathbf{V}-K_h\nabla^2T=0 \\ p=\rho RT \end{aligned}\right\}. \tag{1}$$

When these equations are subjected to: (i) a perturbation, $\mathbf{V}=V+v$; (ii) an axis orientation such that $\partial/\partial x\equiv 0$ (in accordance with observations); (iii) a subtraction of the mean flow; (iv) the Boussinesq approximation; and (v) non-dimensionalization using arbitrary characteristic time, length and velocity

Unauthenticated | Downloaded 08/03/24 07:12 AM UTC

scales, the following set results:

$$\left.\begin{aligned}
\chi u_t + Vu_y - \psi_y U_z - \frac{1}{\mathrm{Ro}}\psi_z - \frac{1}{\mathrm{Re}}\nabla^2 u = 0 \\
\chi \psi_{zt} + V\psi_{zy} - \psi_y V_z + \frac{1}{\mathrm{Ro}}u - \frac{1}{\mathrm{Re}}\nabla^2\psi_z + Dp_y = 0 \\
\chi \psi_{yt} + V\psi_{yy} + g_0(T/\bar{T}) - \frac{1}{\mathrm{Re}}\nabla^2\psi_y - Dp_z = 0 \\
\chi T_t + VT_y - \psi_y\theta_z - \frac{1}{\mathrm{RePr}}\nabla^2 T = 0
\end{aligned}\right\}, \quad (2)$$

where $v=\psi_z$, $w=-\psi_y$, ψ a streamfunction, $V(\infty)=V_g$, $V(0)=0$, $u(\infty)=U(0)=0$; $\chi=L/V\Upsilon$, $\mathrm{Ro}=V_g/fL$, $\mathrm{Re}=VL/K_m$, $D=P_0/\rho_0 V_g^2$, $\mathrm{Pr}=K_m/K_h$, $g_0=gL/V_g^2$; and θ_z is the non-dimensional potential temperature gradient, $(T_z+g/c_p)(L/\Delta T_0)$.

Since a characteristic length or time scale does not enter this set, appropriate scales must be selected from those available by combination of the parameters which enter through the equations and the boundary conditions. Specifically, these are, together with their fundamental units, $f(1/\Upsilon)$, $V_g(L/\Upsilon)$ and $K(L^2/\Upsilon)$, where Υ is time. The parameter D clearly involves only the pressure terms and can be eliminated by redefining pressure, or cross-differentiation. Gravity enters only through the buoyancy term, thus does not appear in the unstratified limit and would not yield appropriate parameters for this limit. This leaves three possible relevant scales each for time and length; these are summarized in the following table together with order-of-magnitude values for typical atmospheric mid-latitude values.

Length		Time	
Parameter	Magnitude	Parameter	Magnitude
K/V	0.1 m	K/V^2	10^{-2} sec
$(K/f)^{\frac{1}{2}}$	100 m	$(K/f)^{\frac{1}{2}}/V$	10 sec
V/f	10^5 m	$1/f$	10^4 sec

The choice of characteristic non-dimensionalizing parameters is arbitrary, and serves to scale the importance of each term by means of the non-dimensional coefficients appearing in the equation. Only when the limit of one of these parameters is taken does the choice of scales become critical, yielding trivial or inconsistent equations when the wrong scale is chosen for a given limit. This becomes evident in the present set of equations, since for all choices of scales, only the single non-dimensional parameter, $\xi=(2Kf)^{\frac{1}{2}}/V_g=1/\mathrm{Ro}=2/\mathrm{Re}$, occurs as a coefficient of different terms in the equations. It may be noted that the choice of characteristic time will involve only the coefficient of the time-dependent inertial term. If no limit is taken, the coefficient will merely enter as a factor in subsequently determined growth rates.

When the parameters $\Upsilon=1/f$ and $L=V/f$ are chosen, and the limit $\xi\to 0$ (inviscid limit) taken, the equations appropriate to geostrophic or inertial flow are obtained. If the characteristic length K/V is adopted, the coefficient ξ^2 appears multiplying the Coriolis term, allowing only the irrotational equations in the $\xi\to 0$ limit, and a trivial equation in the $\xi\to\infty$ limit. When the length scale appropriate to the Ekman layer, $\delta=(K/f)^{\frac{1}{2}}$, is used, equations which include the Ekman equations in the $\xi\to\infty$, steady-state limit are obtained. To retain the growth term in the $\xi\to 0$ limit of these equations, the time scale L/V_g is chosen for the non-dimensionalization:

$$\left.\begin{aligned}
u_t + Vu_y - \psi_y U_z - \frac{\xi}{2}\nabla^2 u - \xi\psi_z = 0 \\
\psi_{zt} + V\psi_{zy} - \psi_y V_z - \frac{\xi}{2}\nabla^2\psi_z + \xi u + Dp_y = 0 \\
\psi_{yt} + V\psi_{yy} - \frac{\xi}{2}\nabla^2\psi_y + g_0 T/\bar{T} - Dp_z = 0 \\
T_t + VT_y - \theta_z\psi_y - \frac{\xi}{2P}\nabla^2 T = 0
\end{aligned}\right\}. \quad (3)$$

This set of four stability equations is an eighth-order set with four unknowns, u, ψ, p and T. A first-order simple-harmonic perturbation of form

$$\begin{Bmatrix}\psi\\ u\\ T\end{Bmatrix} = \begin{Bmatrix}\phi\\ \mu\\ \tau\end{Bmatrix}\exp[i\alpha(y-ct)]$$

is assumed, where α is the wavenumber and c the complex eigenvalue, with real part the wave velocity and imaginary part the growth ($c_i>0$) or decay factor. After the pressure terms have been eliminated by cross-differentiation, the following basic set results:

$$\left.\begin{aligned}
\{(V-c)\phi'' - [V''+\alpha^2(V-c)]\phi \\
\quad - \xi(\phi'''' - 2\alpha^2\phi'' + \alpha^4\phi)/(i\alpha 2)\} \\
\quad + (\xi/i\alpha)\mu' + (g_0/\bar{T})\tau = 0 \\
(V-c)\mu - U'\phi - \xi(\mu'' - \alpha^2\mu)/(i\alpha 2) - (\xi/i\alpha)\phi' = 0 \\
(V-c)\tau - S\bar{T}\phi - \xi(\tau'' - \alpha^2\tau)/(i\alpha 2\mathrm{Pr}) = 0
\end{aligned}\right\}, \quad (4)$$

where $S=\theta_z/\bar{T}$.

The equations now consist of (i) the combined v and w momentum equations, defining the streamfunction parameter; (ii) the u momentum equation, coupled via the Coriolis force terms; and (iii) the heat equation, coupled via the buoyancy term. When τ is eliminated and the operator $D=\partial/\partial z$ is used, the perturbation

Unauthenticated | Downloaded 08/03/24 07:12 AM UTC

equations in their most condensed form can be written

$$\left.\begin{aligned}
&\left\{\left[(D^2-\alpha^2)-\frac{i2\alpha\mathrm{Pr}}{\xi}(V-c)\right]\left[(D^2-\alpha^2)^2\right.\right.\\
&\left.\left.-\frac{i2\alpha}{\xi}(V-c)(D^2-\alpha^2)+\frac{i2\alpha}{\xi}V''\right]-\alpha^2\mathrm{Ra}\right\}\phi\\
&-\left\{\left[(D^2-\alpha^2)-\frac{i2\alpha\mathrm{Pr}}{\xi}(V-c)\right](2D)\right\}\mu=0\\
&\left[(D^2-\alpha^2)-\frac{i2\alpha}{\xi}(V-c)\right]\mu+2\left(D+\frac{i\alpha U'}{\xi}\right)\phi=0\\
&\mathrm{Ra}\equiv\frac{-4\mathrm{PrRi}}{\xi^2}=\frac{g(\bar{T}_z+g/C_p)\delta^4}{\bar{T}K_hK_m}\\
&\mathrm{Ri}=\frac{g}{\bar{T}}\frac{(\bar{T}_z+g/C_p)}{(V/\delta)^2}\\
&\xi=(2Kf)^{\frac{1}{2}}/V_g=\delta f/V_g=1/\mathrm{Ro}=2/\mathrm{Re}
\end{aligned}\right\}\quad(5)$$

While it is possible to solve the entire eighth-order set, there is a large proliferation of terms in the explicit form of (5), and a significant computational time involved per case. Thus, the direction taken was to seek comprehensive solutions of the lower order equations resulting when various terms are neglected in (5). A second-order equation is obtained by neglecting Coriolis and viscous terms, and a sixth-order equation by neglecting the Coriolis terms only. The sixth-order set with the Ekman velocity profile parameter and neglecting stratification terms only was solved by Lilly (1966). The fourth-order equation obtained by neglecting Coriolis and stratification is the Orr-Sommerfeld equation with the Ekman velocity profile as a parameter. In this paper, the Coriolis terms only have been neglected. Although the instability under investigation is an inviscid type, it is necessary to add the viscous terms in order to obtain a non-singular equation.

I. No Coriolis effect

$$\left\{\left[(D^2-\alpha^2)-\frac{i2\alpha\mathrm{Pr}}{\xi}(V-c)\right]\left[(D^2-\alpha^2)^2\right.\right.$$
$$\left.\left.-\frac{i2\alpha}{\xi}(V-c)(D^2-\alpha^2)+\frac{i2\alpha}{\xi}V''\right]-\alpha^2\mathrm{Ra}\right\}\phi=0.\quad(6)$$

II. Neutral stability, no Coriolis effect (Ri=0, Pr=∞)

$$\left[(V-c)(D^2-\alpha^2)-V''-\frac{\xi(D^2-\alpha^2)^2}{i\alpha 2}\right]\phi=0.\quad(7)$$

III. $\xi\to 0$ (inviscid, no Coriolis effect)

$$\left\{D^2-\left[\alpha^2+\frac{V''}{V-c}-\frac{\mathrm{Ri}}{(V-c)^2}\right]\right\}\phi=0.\quad(8)$$

The explicit form of the sixth-order eigenvalue equation is

$$\begin{aligned}
&\phi''''''-3\alpha^2+i(1+\mathrm{Pr})\alpha\mathrm{Re}(V-c)\phi''''+2i\alpha\mathrm{Re}U'\phi'''\\
&-3\alpha^4-2i\alpha^3\mathrm{Re}(V-c)(1+\mathrm{Pr})+(V-c)^2\alpha^2\mathrm{Re}^2\mathrm{Pr}\phi''\\
&-2i\alpha\mathrm{Re}(\alpha^2V'+V''')\phi'+[\alpha^6+i\alpha^5\mathrm{Re}(\mathrm{Pr}+1)(V-c)\\
&-\alpha\mathrm{Re}V''''-(V-c)^2\alpha^4\mathrm{Re}^2\mathrm{Pr}-(V-c)\alpha^2\mathrm{Re}^2\mathrm{Pr}V''\\
&+\alpha^2\mathrm{Re}^2\mathrm{PrRi}]\phi=0,\quad(9)
\end{aligned}$$

i.e.,

$$\phi''''''+K_1\phi''''+K_2\phi'''+K_3\phi''+K_4\phi'+K_5\phi=0.$$

The neutral characteristic equation is obtained in the Ri$\to$0, Pr$\to\infty$ limit for this equation.

Results for the sixth-order, viscous stratified equation were calculated using the shooting method. The solutions to the fourth-order equation have been presented previously (Brown, 1970). Solutions to the second-order equation were calculated using the same method, anticipating difficulties in the vicinity of the critical layer and neutral stability.

The lateral velocity parameter, $V(z)$, will vary according to the type of flow considered. The Ekman solution provided systematically variable analytic profiles with orientation angle ϵ. This angle is chosen such that $\partial/\partial x=0$, in accordance with the many observations of the two-dimensional nature of the perturbation. Thus, it is the angle, positive in a counterclockwise sense, between the geostrophic velocity and the x (or roll) axis. Consequently, $V(z)$ is the component of mean velocity in a plane oriented $\epsilon+90°$ counterclockwise to $\mathbf{V}_g$.

b. Method of solution

The shooting method of solution can conveniently be used for the boundary value problems defined by (6), (7) and (8). In this method one assumes sufficient boundary conditions at one boundary, and for a given set of parameters [$V(z)$, α, ξ, Ri], an eigenvalue c is guessed, and the equation can be integrated. In this way a functional relationship arises between the assumed eigenvalues and the residues obtained from the difference between the integrated solution and the condition to be satisfied at the other boundary. The roots of this function then provide the eigenvalues and corresponding eigenfunctions which satisfy both boundary conditions. The condition of complete smoothness at the free stream boundary provides sufficient boundary conditions for the integration. A check revealed the solutions to be insensitive to the redundant boundary conditions at this boundary. A complete description of the shooting method is given in Brown and Lee (1972).

Unauthenticated | Downloaded 08/03/24 07:12 AM UTC

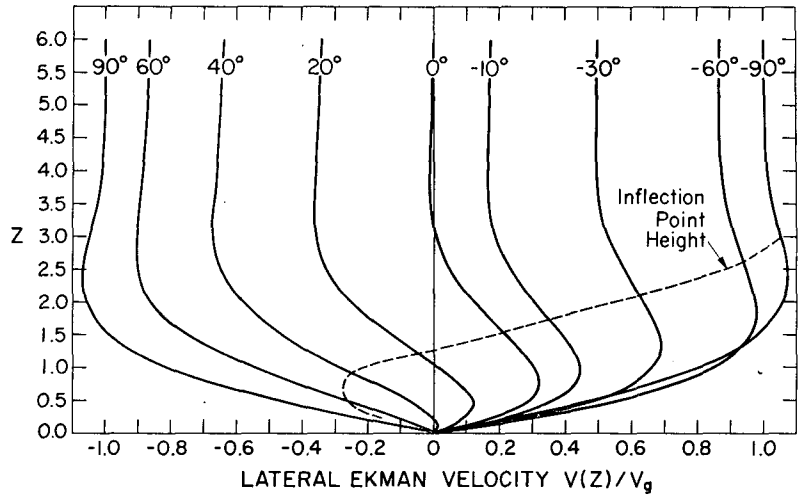

FIG. 1. Two-dimensional velocity profiles taken in vertical planes normal to the roll direction. The angle ϵ denotes the roll angle to the left of the geostrophic velocity. The height and velocity are given in increments of δ and V_g, respectively.

3. Results

The contention of this paper is that the sixth-order equations are sufficient to define the roll instabilities of the stratified Ekman velocity profile at supercritical Reynolds numbers. One might expect the $\xi \to 0$ limit to produce appropriate solutions in this case; however, the singular nature of the resulting equation precludes this. In addition, the solutions to the second-order equation are physically significant only if it represents as asymptotic limit of the singularly perturbed viscous solution. There are also practical difficulties arising with the singular equation associated with the continuous spectrum of solutions, which tend to obscure the discrete mode. Nevertheless, using the hindsight of the higher order solutions, the shooting method may be used with the inviscid equation to conveniently investigate the modes which have been established as solutions of the nonsingular viscous equation. While this procedure was successful in relating the sixth-order solutions to the fourth order (the $\mathrm{Ri} \to 0$ limit), the second-order results for maximum growth rate parameters did not correspond well to the higher order solutions. However, the second-order solutions were qualitatively similar, with similar eigenfunctions, and the viscous solutions were independent of Reynolds number for $\mathrm{Re} > 500$. The significant differences in eigenvalues could be partly ascribed to the slightly different computational methods, since the step is probably too large for a second-order integration, whereas a Gram-Schmidt purification scheme could be employed with the higher order equations to forestall growth of the computational error.

Accordingly, the known instability mode for the

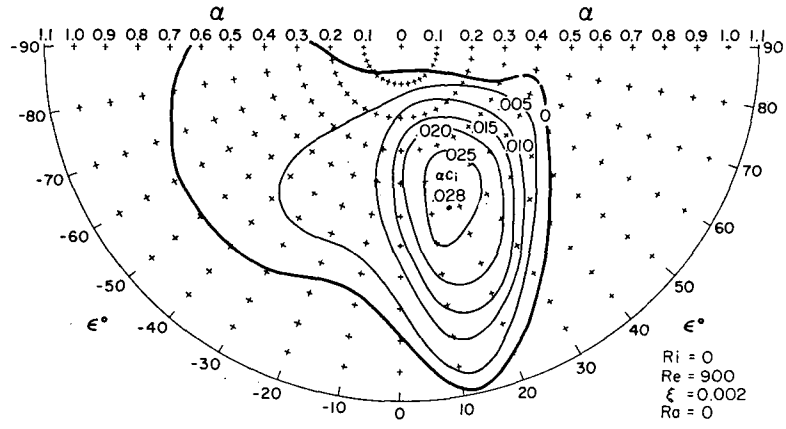

FIG. 2. Growth rate curve for the neutral Ekman layer as a function of wavenumber α and orientation angle ϵ. A maximum growth rate of 0.028 occurs at wavenumber 0.5 oriented 18° to the left of the geostrophic velocity. All quantities are non-dimensionalized with respect to δ and V_g.

Unauthenticated | Downloaded 08/03/24 07:12 AM UTC

Ekman layer, obtained from the viscous solution, is considered. In this case, the instability wave associated with the eigenvalue c will depend upon the wavenumber α, the Reynolds number—or dimensionless parameter ξ—and the velocity profile $V(z)$. In a turning wind, the mean wind profile "confronted" by the two-dimensional perturbation will vary according to its orientation. Thus, in the case of the Ekman profile, perturbations traveling parallel to the geostrophic flow ($\epsilon \rightarrow \pm 90°$) must grow with respect to a strong shearing wind, with weak inflection points in the upper part of the profile, whereas perturbations with longitudinally oriented axes ($\epsilon \rightarrow 0$) "see" less shear and stronger inflection points (Fig. 1). The stability curves obtained from the unstratified fourth-order equations are identical to those obtained in the limit $\mathrm{Ri} \rightarrow 0$ from the stratified sixth-order equation (Fig. 2). It is then relatively easy to trace this mode in the sixth-order equation for different Ri using the shooting method.

a. Variable Ri

The Richardson number used to this point is the bulk value, depending upon a temperature gradient (constant) and a mean velocity gradient over the entire region. Although consistent usage of this parameter is not erroneous, it would seem to lack some physical significance in that a mean velocity gradient poorly describes some of the profiles. If this Richardson number is considered variable such that $\mathrm{Ri}=\mathrm{Ri}_b$ for the layer below a critical height Z_c, and $\mathrm{Ri}=\mathrm{Ri}_u$ above z_c, then the maximum growth rate is found to depend upon z_c as in Fig. 3. Although significantly different Richardson numbers above or below the inflection point height may affect the vertical structure and phase of the eigenfunction, the critical parameters for the maximum growth rate depend upon the Richardson number in the vicinity of the inflection point. Hence, a local Ri based upon the temperature and component velocity gradients at the inflection point height has been calculated. This qualitative result also appears

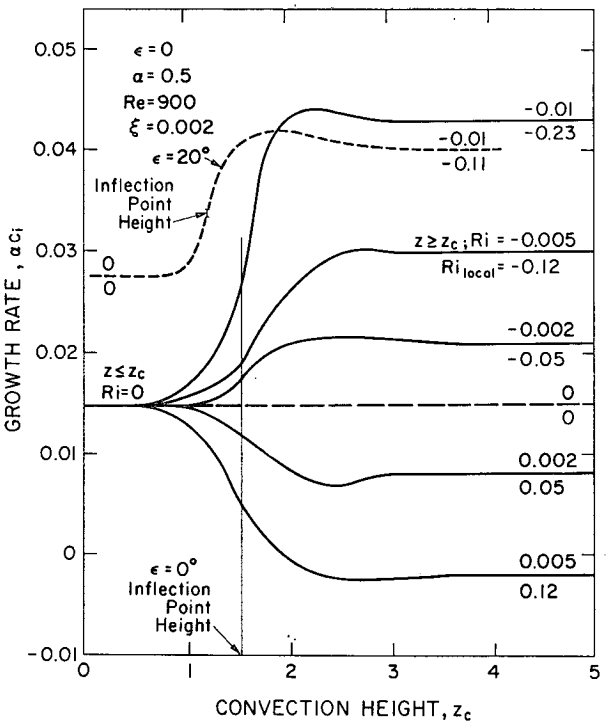

FIG. 3. Growth rate curves for a two-step Richardson number, $\mathrm{Ri}=\mathrm{Ri}_d$ (labeled on curves) for $z<z_c$, and $\mathrm{Ri}=0$ for $z>z_c$. Both the bulk Ri and local Ri_l are shown. For example, when $\mathrm{Ri}=-0.01$ up to $z_c=2$, and $\mathrm{Ri}=0$ for $z>2$, αc_i corresponds to $\mathrm{Ri}=-0.01$ values.

from the second-order equation results, where the jump in growth rate is steeper, being unmodulated by the effects of viscosity.

The effect of stratification on this mode is shown in Figs. 4–6. As stratification is increased, the maximum growth rate position shifts to roll orientations up to 30° to the left of the upper boundary velocity. Wavelengths remain fairly constant at $\lambda=4\pi\delta$. The mode is completely extinguished at $\mathrm{Ri}=0.02$. The maximum Ri_l is <0.25. This compares with the well known

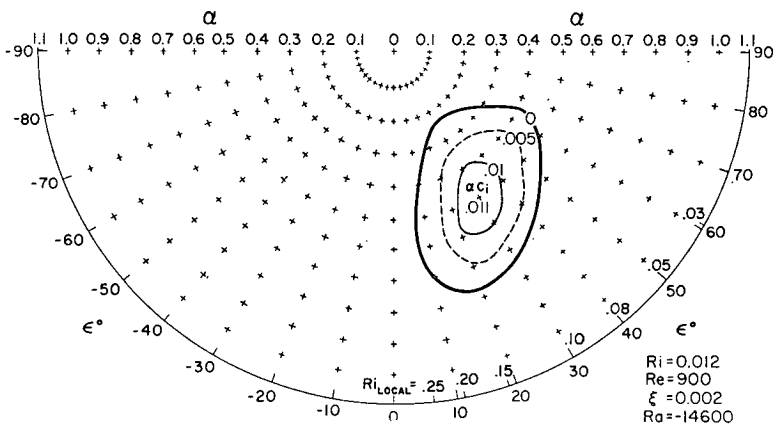

FIG. 4. Growth rate curves for the inflection point mode at a bulk $\mathrm{Ri}=0.012$.

Unauthenticated | Downloaded 08/03/24 07:12 AM UTC

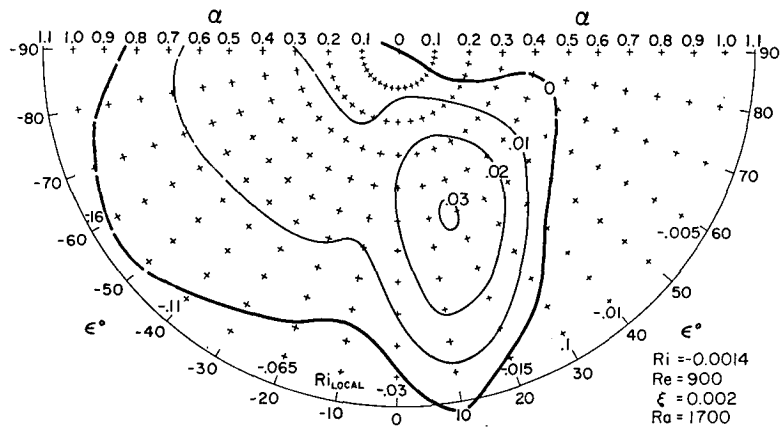

FIG. 5. Growth rate curves for the inflection point mode at a bulk $\mathrm{Ri}=-0.0014$.

inviscid result (e.g., see Miles, 1960) since the ratio of velocity gradient at the critical layer (where $V=c_r$) to that at the inflection point is nearly unity. The stability diagrams at negative bulk Richardson numbers show the critical orientation angle moving toward 0° and shorter wavelengths (Fig. 7). For even small negative Richardson numbers, the buoyancy effect has broadly amplified the weak instability region at large negative ϵ in addition to the maximum growth rate. The convective mode did not appear as a separate instability at these Reynolds numbers. The buoyant energy is apparently channeled into increased growth rates for the dynamic mode.

The complete lateral streamfunction ψ for maximum growth rate is shown in Figs. 8–10. These cross sections of the perturbation flow indicate the familiar roll cells. When superimposed on the mean flow, a helical flow results. Negative stratification reduces the tilt of the cells for $z/\delta<1$, whereas positive stratification increases the tilt, mainly in the vicinity of the inflection point height ($z=1.3$). Since increased tilt is associated with perturbation phase relations favoring energy transfer from mean flow to perturbation in the inflection point mechanism, these results reflect the effect of thermal energy input. The growth rates vs Ri as a function of ϵ are plotted in Fig. 11 for the critical inflection point wavenumber. The local Richardson number depends on the component velocity gradient at the inflection point, hence upon ϵ. The growth rate is increased for all ϵ by negative stratification. The increase generally reflects corresponding decreases in Ri_l.

4. Discussion

The complete stability set of equations (5) for the geophysical boundary layer present an eigenvalue problem with the complex eigenvalue c, determined as a function of α, $V(z)$, $U(z)$, $T(z)$, ξ, Pr and Ra. It is possible to numerically solve this eighth-order set employing the shooting method with simultaneous integration of the equations. However, the attendant abundance of parameters of this set, plus the limiting forms of the equations suggested by the scaling analysis, prompted a detailed investigation of these limit

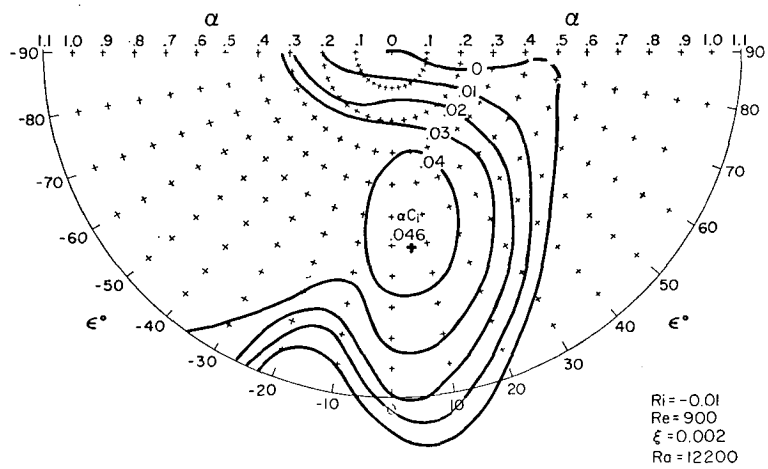

FIG. 6. Growth rate curves for the inflection point mode at a bulk $\mathrm{Ri}=-0.01$.

Unauthenticated | Downloaded 08/03/24 07:12 AM UTC

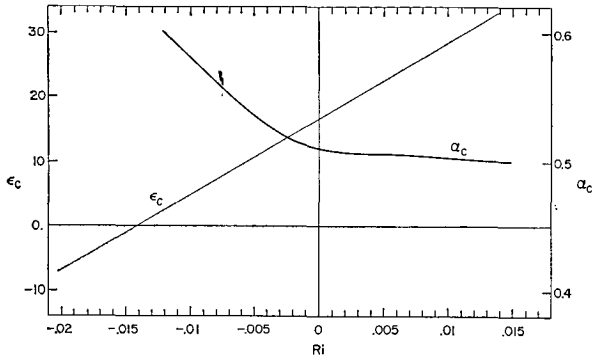

FIG. 7. The behavior of wavenumber and orientation angle at maximum growth rates vs Ri.

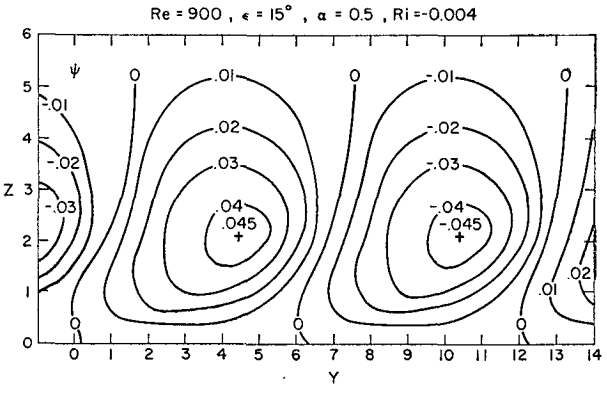

FIG. 9. Same as Fig. 8 for Ri = −0.004.

equations. In addition, a successful parameterization of the geophysical stability problem requires the existence of a physically realistic limit equation solution. This limit can be realized by an appropriate nondimensionalization and the careful consideration of the limiting behavior of pertinent variables. Such limits are usually singular perturbations on the complete set, dropping the order of the governing equations and, consequently, the number of boundary conditions which can be satisfied. Hence, care must be exercised in interpreting the results.

By considering that $\xi = (2Kf)^{\frac{1}{2}}/V_g \approx 10^{-3}$ in the atmosphere, the limit for $\xi \to 0$ was considered [Eq. (8)], reducing the parameters to only the eigenvalue, wavenumber, velocity profile and its second derivative, and the Richardson number. This would appear to be a necessary approximation if a successful parameterization of the stratified stability problem is to be accomplished. It eliminates the implied sensitivity of the convective instability on the vertical scaling parameter δ, which is physically unattractive in view of the indefinite nature of δ. Nevertheless, the $\xi = 0$, second-order equation and the viscous fourth- and sixth-order equations imply that stability depends upon the mean velocity profile and its second derivative, requiring fairly detailed knowledge of the mean velocity profile.

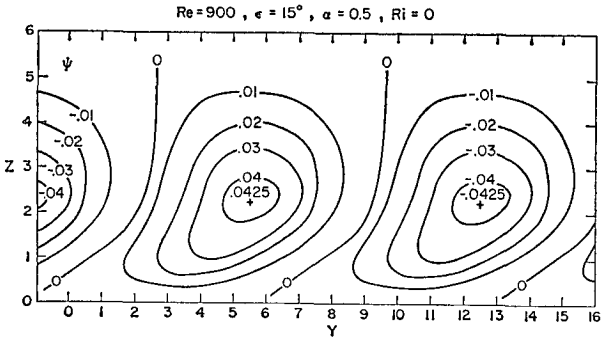

FIG. 8. Constant values of the streamfunction ψ for Ri = 0, and typical maximum growth rate values for ϵ and α. Coordinates z and y have been non-dimensionalized by δ.

This dependence is revealed to be weak, however, by the qualitative similarity of the results for a wide range of velocity profiles. The implied indifference of the solutions in the $\xi \to 0$ limit is realized in the numerical solutions, where the growth rate figures, presented for $\xi = 0.002$, do not change for either mode as ξ decreases.

Unfortunately, the $\xi = 0$ limit is highly singular, dropping the equations from eighth order to second order, resulting in an equation which is itself singular in the ranges of interest. Solutions to such an equation are physically realistic only if they represent the asymptotic limit of solutions for the higher order nonsingular equation. The singularity can be removed by adding the viscous terms. This is related to the fact that viscosity forces, in addition to being important at the boundary, are significant in the vicinity of the critical layer, where $V = c$.

The fourth-order neutrally stratified equation yielded one unstable eigenvalue for each set of parameters which was clearly associated with the inflection point, the phase velocities of the eigenvalue closely following the mean velocity at the inflection point height. However, the infinity of inflection points associated with an analytic Ekman profile would provide a theoretical "layering" of eigenvalue modes in Fig. 2. By considering the profiles of Fig. 1, one can see that the inflection point occurs at $z = 0$ for $\epsilon = 90°$, moving progressively upward to $z = \pi$ at $\epsilon = -90°$. In view of the extremely small growth rates and the unlikely possibility of such

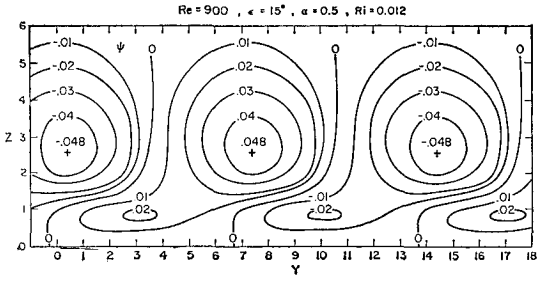

FIG. 10. Same as Fig. 8 for Ri = 0.012.

Unauthenticated | Downloaded 08/03/24 07:12 AM UTC

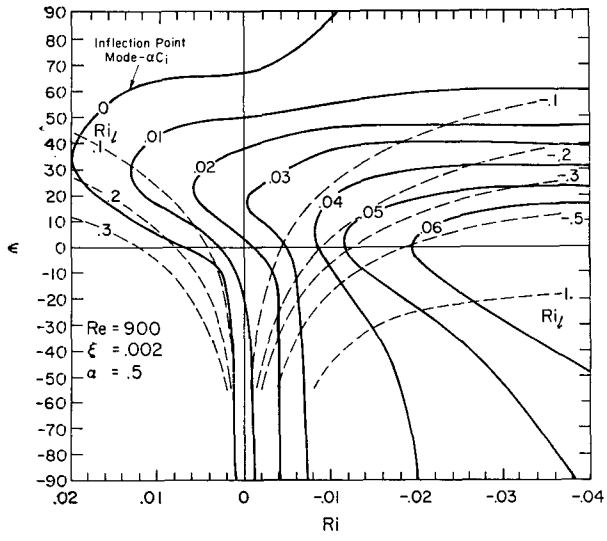

FIG. 11. Growth rates as a function of ϵ and Ri. The local Richardson numbers at the inflection point height are given by dashed lines labeled Ri_l.

details of the mean profile being developed in the geophysical boundary layer, the upper inflection points were arbitrarily suppressed. The program was unable to resolve the inflection point as $\epsilon \to 90°$ where the inflection point height $\to 0$. With sufficient resolution, the neutral stability curve could be expected to approach 90° at $\alpha \approx 0.4$.

It might be pointed out here that only a two-dimensional perturbation has been considered, corresponding to observational and experimental data. The U momentum equation is not involved in the roll instability solution, unless Coriolis forces are included. When the Coriolis terms are included, they bring $U'(z)$ as an additional parameter into the stability analysis in (5). The $U(z)$ profile at $\mp\epsilon$ corresponds to the $V(z)$ profile in Fig. 1 at $\epsilon \pm 90°$. Thus, there exists the potential for an inflection point instability in the U profile as a source of energy. In particular, this inflection point has a different velocity gradient, hence a different Ri_l, e.g., at $\epsilon = -30°$, a $Ri_l = 0.25$ based on $V(z)$ has a corresponding $Ri_l = 0.011$ at the $U(z)$ inflection point. This feature is not sufficient to explain all of the instabilities appearing in the provocative results obtained by Kaylor and Faller (1972), as some cases exhibit positive growth rates with both $Ri_l > 0.25$. However, in many cases, the phase velocity is associated with the high shear region of the $U(z)$ profile rather than the inflection point velocity, e.g., $c_r = 0.509$ at $\epsilon = 0°$ (the U profile corresponds to the 90° curve in Fig. 1). Hence, a Ri_l may be much smaller. The basic energy source then must arise from another source, perhaps the viscous mechanism as discussed by Lin (1955). It is apparent that resonance alone is insufficient to allow growth for $Ri_l > 0.25$ since the resonant phase speed, $c_r = 0.5$, equals the velocity at the V profile inflection point for $\epsilon = -21°$, yet no growth occurs here for $Ri_l > 0.25$. The need for the Coriolis coupling implies a dependence on the $U(z)$ profile and the various Richardson numbers which is in need of further exploration. In any event, for the purpose of this paper, the scaling analysis clearly indicates that this coupling disappears at high Reynolds numbers (also see Barcilon, 1965).

Although the basic mode investigated in the sixth-order equation reduced to the fourth-order results of Fig. 2 in the $Ri \to 0$ limit, the computations were complicated by the occurrence of spurious modes. These modes could be identified as computational through their dependence on the step size in the Runge-Kutta integration procedure, or inferred from an independence of Ri, with no corresponding solution in the fourth-order set. The $Ri = 0$, $Pr \to \infty$ limit, which produces the fourth-order neutral equations from the sixth-order stratified set is well behaved with respect to these modes, or vice versa. A value of $Pr = 0.7$ was used, however, for which the solutions were essentially independent of Pr. The results were independent of depth for $z/\delta > 6$.

The effect of stratification upon maximum growth rate parameters, ϵ_c and α_c, includes a trend toward shorter wavelengths and small orientation angles for unstable stratification. The stable stratification effect upon these values is small and probably insignificant compared to the general damping, which will include the small-scale turbulence and hence a decreased eddy viscosity coefficient.

The extension of the instability modes into the highly convective state is needed. As usual, the first indications of the modes associated with the resulting dynamic/convective instability interaction appeared in the investigations of Faller and Kaylor (1967). However, this extension to the results of this paper will require significant refinements in the present program. Also, previous results (Brown, 1970) have shown the possibility of a finite perturbation equilibrium state for the dynamic instability (secondary rolls in a modified mean flow). Thus, it is felt that a complete description of the convective mode is likely to require this variable mean flow.

The analysis in this paper applies to a fluid flow at supercritical Re ($\gtrsim 400$) where the stratification change is significant. For an atmospheric analog, it is necessary to have an eddy viscosity parameterization of the small-scale turbulence. This is at best a rough process, and use of a constant mean value is an adequate first approximation provided the results are not critically dependent upon the profile shape. Since the instability could be expected to set in as the turning profile was developing, the exact Ekman spiral is not likely to become established. Indeed, the entire atmospheric analog depends upon a relative insensitivity to the mean parameters in accordance with the indefinite values obtainable in meteorological measurements.

Unauthenticated | Downloaded 08/03/24 07:12 AM UTC

The results presented here appear to substantiate the conclusion that the qualitative nature of the roll instability is characteristic to a wide band of atmospheric or oceanic parameters.

Acknowledgments. Support during this work was obtained from the National Science Foundation under Grant GA 1099 and from the National Center for Atmospheric Research.

REFERENCES

Asai, T., 1969: Stability of a plane parallel flow with variable vertical shear and unstable stratification. NCAR MS 69-194, National Center for Atmospheric Research, Boulder, Colo.

Barcilon, B. 1965: Stability of non-divergent Ekman layers. *Tellus*, **17**, 53–68.

Benny, D. J., 1960: A nonlinear theory for oscillations in a parallel flow. *J. Fluid Mech.*, **10**, 209–236.

Brown, R. A., 1970: A secondary flow model of the planetary boundary layer. *J. Atmos. Sci.*, **27**, 742–757.

——, and F. Lee, 1972: On the shooting method applied to the rotating stratified boundary layer stability problem. *J. Comput. Phys.* (in press).

Etling, D., 1971: The stability of an Ekman boundary layer flow as influenced by the thermal stratification. *Beitr. Phys. Atmos.*, **44**, 168–186.

Faller, A., and R. Kaylor, 1967: Instability of the Ekman spiral with application to the planetary boundary layers. *Phys. Fluids Suppl.*, **10**, 212–219.

Gage, K. S., and W. H. Reid, 1968: The stability of thermally stratified plane Poiseuille flow. *J. Fluid Mech.*, **33**, 21–32.

Gallagher, A. P., and A. M. Mercer, 1965: On the behavior of small perturbations in plane couette flow with a temperature gradient. *Proc. Roy. Soc. London*, **A286**, 117–128.

Kaylor, R., and A. Faller, 1972: Instability of the stratified Ekman boundary layer and the generation of internal waves. *J. Atmos. Sci.*, **29**, 497–509.

Koppel, D., 1964: On the stability of flow of a thermally stratified fluid under action of gravity. *J. Math. Phys.*, **5**, 963–982.

LeMone, M., 1972: Structure and dynamics of horizontal roll vortices in the planetary boundary layer. Ph.D. thesis, University of Washington.

Lilly, D. K., 1966: On the instability of Ekman boundary flow. *J. Atmos. Sci.*, **23**, 481–494.

Lin, C. C., 1955: *Theory of Hydrodynamic Stability*. Cambridge University Press, 155 pp.

Maslowe, S. A., and J. Thompson, 1971: Stability of a stratified free shear layer. *Phys. Fluids*, **14**, 453–458.

Miles, J. W., 1960: On the stability of heterogeneous shear flow. *J. Fluid Mech.*, **10**, 496–508.

Ogura, Y., and A. Yagihashi, 1969: A numerical study of convective rolls with a flow between horizontal parallel plates. *J. Meteor. Soc. Japan*, **47**, 205–217.

Unauthenticated | Downloaded 08/03/24 07:12 AM UTC